The spatial structure of the lowest ion-acoustic instability modes in the high-current discharge of CW argon ion lasers

V I Donin[1]**, V A Ivanov**[1]**, V V Pickalov**[2] **and D V Yakovin**[1]

[1] Institute of Automation and Electrometry, Siberian Branch of the Russian Academy of Sciences, Novosibirsk 630090, Russia
[2] Institute of Theoretical and Applied Mechanics, Siberian Branch of the Russian Academy of Sciences, Novosibirsk 630090, Russia

E-mail: donin@iae.nsk.su

Abstract
The cross-sectional structure of the two lowest ion-acoustic instability modes in the positive column of a cylindrical, high-current discharge, traditionally used as an active medium in CW ion gas lasers, has been investigated. The diameter and length of the discharge column in our experiments were 16 mm and 1 m, respectively, and the discharge current was 250–350 A. Under these conditions, the observed mode frequencies were $\nu_1 = 190$ kHz and $\nu_2 = 390$ kHz. To obtain the spatial structure of these modes, time-resolved integral projections of spontaneous argon-plasma emission were measured in planes normal to the discharge axis. From the power spectra of the measured projections, the structures of the modes ν_1 and ν_2 were reconstructed using computerized tomography algorithms. Based on available theoretical models of the instability, the modes have been identified as the (1, 1) and, tentatively, the (1, 2) modes of oscillation.

1. Introduction

In the positive column of low-pressure gas discharges, along with high-frequency ion-acoustic oscillations emerging at frequencies $\omega \lesssim \Omega_i$ (where Ω_i is the ion plasma frequency), low-frequency oscillations with frequencies $\omega \lesssim 10^{-2}\Omega_i$ can also be excited [1–10]. These oscillations arise as the discharge current exceeds a certain critical value, which depends on the discharge conditions. At supercritical currents, the oscillations can be rather intense. This causes damage to the discharge-tube walls, which circumstance obviously imposes limitations on the maximum output power and lifetime of ion lasers [3, 9], including transverse-flow lasers with high-speed gas flows [10].

The low-frequency spectrum of the argon-plasma oscillations in laser discharge tubes, ranging in diameter from 5 to 30 mm, displays several peaks in the frequency region $0.1 \lesssim \nu \lesssim 2$ MHz ($\nu = \omega/2\pi$). Donin *et al* [8] showed that the observed frequencies refer to the lower normal modes of ion-acoustic instability in a wall-confined plasma. The dispersion relation experimentally established for the lowest mode [11] were found to agree fairly well with the theoretical treatment of ion-acoustic oscillations in cylindrical, low-pressure discharges given by Woods [12] and Ewald *et al* [13].

To the best of our knowledge, the only study in which qualitative evidence for the difference between spatial distributions of two lowest modes were obtained experimentally is our previous work [8]. However, the data obtained in [8] were insufficient for the spatial structure of the modes to be determined. The latter goal was pursued in this study using a new oscillatory emission tomography method. Based on the newly obtained data and available theoretical models, we tentatively identify examined modes.

2. Experimental set-up and results

The argon plasma was produced by a continuous high-current discharge ignited in a 1 m long tube with diameter $d = 16$ mm
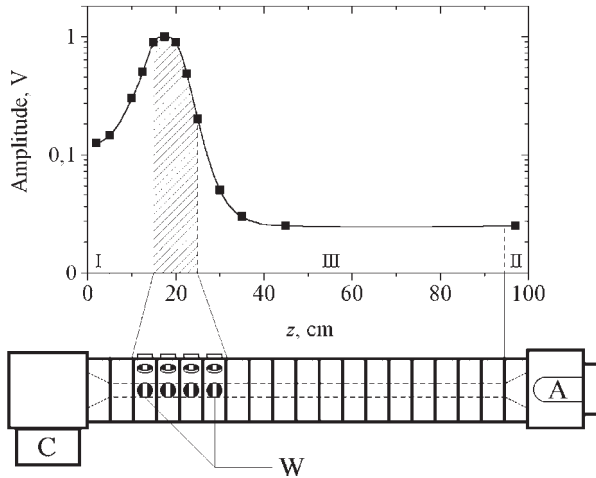
Figure 1. Discharge tube (C—cathode, A—anode) with windows W used to diagnose the plasma (bottom), and the oscillation-amplitude profile measured along the discharge axis z (top); I and II—conical regions of the discharge, III—cylindrical positive column with the optically diagnosed region (shaded area).

(figure 1). The tube, which incorporated a cold arc cathode with a self-heated refractory bush, consisted of water-cooled aluminium sections covered with an oxide film [9]. To allow observation of the plasma emission from the discharge tube, four sections of the tube had 4×16 mm^2 slit-windows oriented perpendicularly to the discharge axis z. Each section had three quartz windows, ensuring viewing angles $\xi = 0°$, $55°$, and $90°$ in several cross-sectional planes normal to the z-axis. The sections fitted with the windows were installed near the cathode, where the oscillations were the most intense. The intensity level of the oscillations was monitored by measuring the potential difference between two neighbouring tube sections. This difference in our experiments did not exceed ± 3 V. Figure 1 (top graph) illustrates the dependence of the measured oscillation amplitude on the z-coordinate. For the initial argon pressure, 0.2–0.4 Torr, in the cold discharge tube (the discharge pressure was much lower, especially in the near-cathode region of the plasma column), the critical current ranged from 250 to 350 A and the total voltage between the electrodes was 140–200 V. Under these discharge conditions, the plasma parameters were the following [9]: the electron density was 10^{14} cm^{-3}, the electron temperature, 5 eV and the ion temperature, 2 eV. At the discharge axis, the plasma contained about 10% of doubly charged ions.

To study the spatial structure of plasma-column oscillations, we used the emission plasma tomography technique [14–16]. The emitted intensity was concentrated in the blue–green portion of the line spectrum of excited singly-charged argon ions, whose concentration was n_i^*. If the excess over the critical current was not too large, the concentration of ions in the ground state was $n_i(t) = n_i + \delta n_i(t)$, where n_i is a steady-state concentration and $\delta n_i(t)$ is a small ($\lesssim 3\%$ of n_i) oscillating additive. In [9], it was shown that under such experimental conditions $n_i^*(t) \propto n_i(t)$ at least for frequencies $\nu < \beta_i$, where β_i is the ionization rate.

The tomographic problem consisted in measuring the plasma emission under different viewing angles in several planes normal to the z-axis. Figure 2 illustrates the
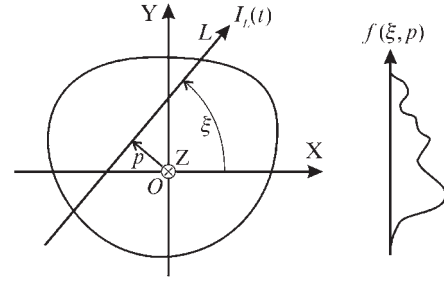

Figure 2. Tomographical geometry.

tomographic geometry used. In this figure, x and y are the coordinates of an observation point in one such plane. The instantaneous intensity $I(t)$ emitted by the argon plasma along an observation ray L is proportional to the line integral of the density of excited ions along the ray trajectory:

$$I_L(t) \propto \int_L n_i^*(x, y, t)\, \mathrm{d}L.$$

In the experiment, we measured integral one-dimensional parallel-beam projections $I(t) \equiv f(\xi, p)$. In the adopted geometry, each beam was uniquely defined by the angle ξ formed by this beam with the axis OX and by the distance p to the z-axis. In the approximation of optically thin plasma, the measured projections are given by the integral Radon transform R [15]:

$$f(\xi, p, t) = R\{n_i^*(x, y, t)\}. \tag{1}$$

From experimentally measured time-dependent projections taken for a set of angles $\xi \in [0, \pi]$, and for a set of coordinates $p \in [-d/2, d/2]$, an estimate of the solution of the integral equation (1) in the form

$$n_i(x, y, t) \propto R^{-1}\{f(\xi, p, t)\} \tag{2}$$

may be obtained, where R^{-1} is an approximation of the inverse Radon transform. A Fourier transform for the variable t may be applied to both parts of expression (2):

$$\tilde{n}_i(x, y, \nu) \propto R^{-1}\{\tilde{f}(\xi, p, \nu)\}, \tag{3}$$

where the tilde over a quantity denotes its Fourier component. The possibility of representing the solution of the inverse problem (2) in the form of a Fourier series was previously validated in [17]. The frequency dependence of $\tilde{n}_i(x, y, \nu)$ at each point of the region of interest represents the spectrum of ion plasma oscillations. For a fixed frequency corresponding to a particular mode, the function $\tilde{n}_i(x, y, \nu)$ represents the spatial distribution of this mode.

The projections and their Fourier spectra were recorded on an experimental set-up shown in figure 3. The radiation emitted from the discharge tube at different viewing angles was converted into an electric signal with the help of an optical system that included a focusing lens, a blue–green light filter, two diaphragms, an optical fibre (see figure 4), and a photomultiplier. In the measurements, two identical systems were used. Each system registered a beam emanating from the discharge tube as a narrow cylinder normal to the discharge axis. The diameters of the diaphragms and the

separation between optical elements were chosen so as to comply with Webb calculations [18]. The spatial resolution of the optical system was 0.25 mm. Each system was mounted on its own bench, whose steady motion along the coordinate p, normal to the z-axis, could be ensured by an electric motor. One of the systems allowed successive measurements of light intensities emitted from two different windows of one and the same discharge-tube section. Since the response time of the multi-channel analog-to-digital converter (ADC) used in our experiments was rather long ($\geqslant 30\,\mu$s), we also used an analog spectrum analyser fed with the pre-amplified output signal of the photomultiplier. The analyser measured the frequency spectrum of the signal. Figure 5 shows a typical spectrum of plasma oscillations that includes a first mode with frequency $\nu_1 = 190\,$kHz and a second mode with frequency $\nu_2 = 390\,$kHz. The bandwidth of the analyser in the treated frequency range was 10 kHz. All measurements

were performed under near-instability conditions. To obtain the spectra of projections, the analyser measured the amplitude of the input harmonic component either at frequency ν_1 or at frequency ν_2. The output signal from the analyser was proportional to the Fourier amplitude and represented the power spectrum of the signal $|\tilde{f}(\xi, p, \nu)|$. The pre-amplified time-averaged signals were also fed to the ADC, each reflecting the dependence of the integral intensity emitted along a particular direction, on the coordinate p. Using these dependences, it was possible to precisely adjust the optical systems. Figure 6 show the typical power spectra of projections measured at the frequencies ν_1 and ν_2. The first-mode projections shows a valley at the centre of the discharge with two peaks of equal amplitudes on either side. Depending on the orientation, the separation between the peaks displayed clear variations (up to their coincidence). The second-mode projections displayed up to three distinct peaks. With the help of a correlator, we measured the cross-correlation function of the oscillations, from which the phase difference between the first-mode maxima was found; this difference turned out to be π rad.

The reconstruction procedure included the determination of the two-dimensional distributions of the emitted intensity from the measured projection dataset with the help of computerized tomography methods and formula (3). To invoke formula (3), it was necessary to individually register in the experiment (or somehow calculate) the imaginary and real parts of the spectrum $\tilde{f}(\xi, p, \nu)$; however, our analyser measured projection power spectra only. In the general case, the shape of a distribution reconstructed from the modulus of a projection dataset spectrum may differ from the spatial structure of the function from which the projections were taken because of the indeterminacy of the phase in the measuring power spectra. The reconstruction error of this algorithm was numerically examined by Ivanov and Pickalov [17]. These authors showed that for many objects usually employed for representation of steady-state harmonic oscillations (including those examined in this study), the algorithm was quite capable of yielding their characteristic spatial structure without substantial distortions.

To reconstruct the tomograms, we used the maximum-entropy technique [15, 19], which proved to be a highly effective tool in solving parallel-beam tomography problems with a small number of available projections. In the computations, the algorithm MENT from the TOPAS-MICRO program package, which was specially designed for solving plasma and gas computerized tomography problems, was used [15]. The reconstructed tomograms of the first-mode oscillations contained two main peaks located symmetrically around the discharge centre (see figure 7(a)). Figure 7(b) shows a typical second-mode tomogram. Because the available projections were few in number, the tomograms displayed small streak artefacts.
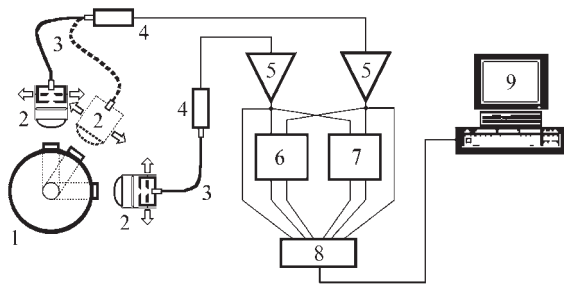

Figure 3. Experimental set-up for studying the spatial structure of plasma oscillations: 1—discharge tube (as viewed along its symmetry axis; the discharge column is shown as a shaded area); 2—optical system with fibre 3 (the arrows show the scanning directions); 4—photomultiplier; 5—amplifier; 6—spectrum analyser; 7—correlator; 8—multi-channel ADC; 9—personal computer.
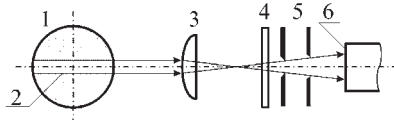

Figure 4. Scheme of the optical system: 1—discharge (cross-sectional view); 2—cylindrical volume element; 3—lens; 4—light filter; 5—diaphragms; 6—fibre inlet plate.
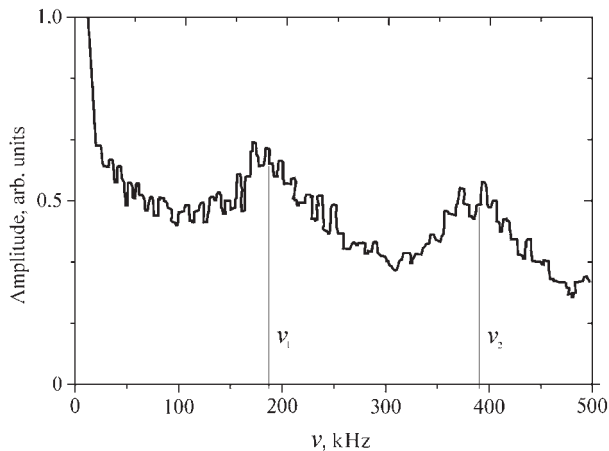

Figure 5. Spectrum of low-frequency ion-acoustic oscillations measured by the analyser under near-instability conditions.

3. Discussion

Unlike the experimental scheme used in [8], the scheme employed in this study allowed investigation of the spatial structure of the discharge-column oscillations by the tomography technique, simultaneously ensuring a much better
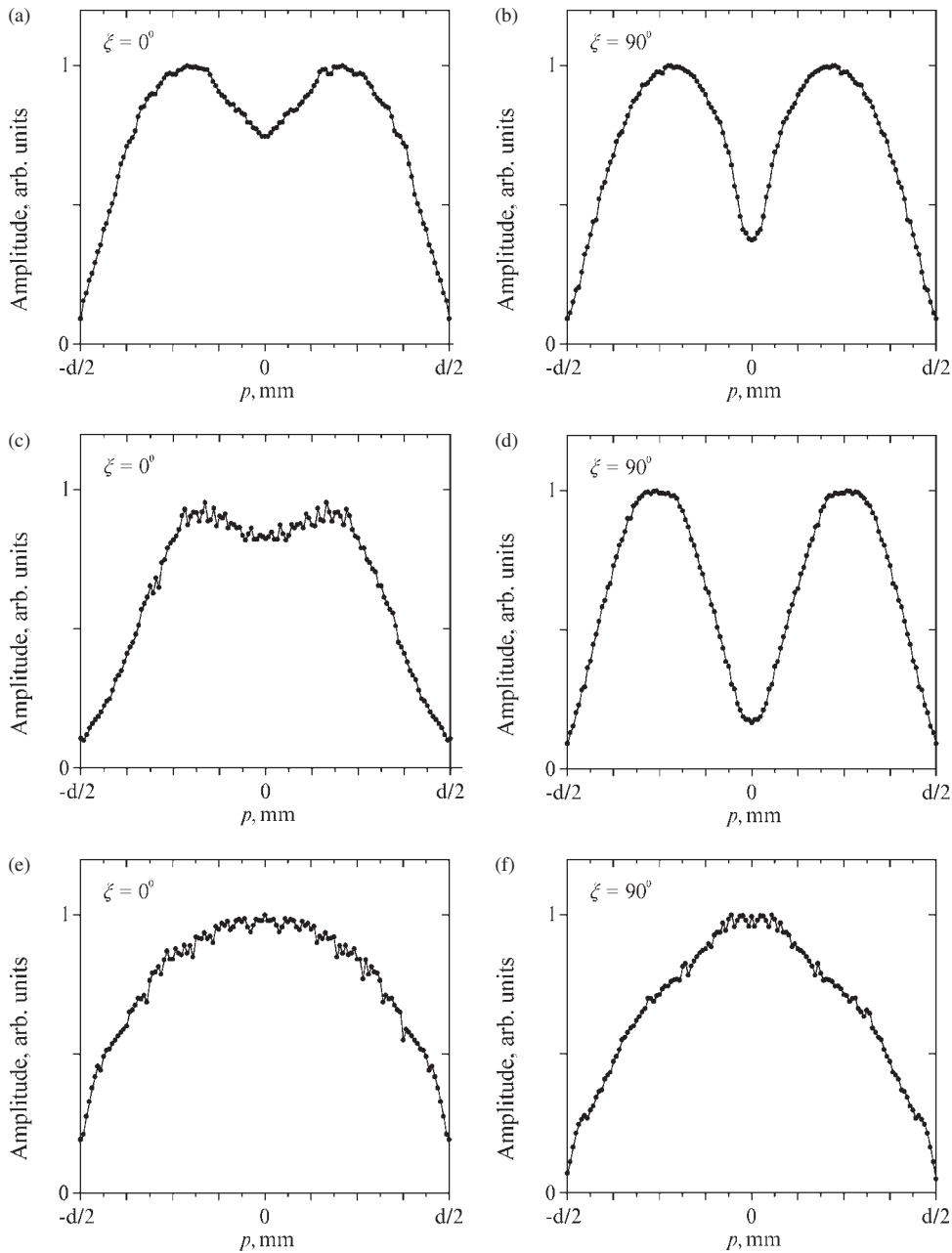
Figure 6. Power spectra of the first-mode (*a*)–(*d*) and second-mode (*e*) and (*f*) projections. The profiles (*c*) and (*d*) were measured in a neighbouring tube section.

spatial resolution. Treating the measured integral-projection power spectra with tomography algorithms, we managed to determine the two-dimensional structure of the two lowest oscillation modes. In turn, examining the measured correlation functions, we revealed the spatial phase non-uniformity of the first mode.

The mode structure of the oscillations in the positive column of the cylindrical discharge was theoretically considered within the framework of hydrodynamic models of ion-acoustic oscillations in [8, 12, 13]. Unlike the models described in [12, 13], the model [8] explains the existence of a discrete spectrum of instability modes. In addition, this model provides a good agreement between predicted and observed mode frequencies. According to [8], the lowest order modes

have the following two-dimensional structure:

$$\delta n_i(r, \varphi) \propto J_m \left(j_{mn} \frac{2r}{d} \right) \cos(m\varphi),$$

where r is the radial coordinate, φ the azimuthal coordinate, and j_{mn} denotes the nth zero of the mth-order Bessel function J_m. Thus, each oscillation mode is uniquely defined by a pair of mode numbers (m, n). The $m = 0$ modes are axisymmetric (purely radial), whereas the modes with $m \neq 0$ are asymmetric.

We have found that the shape of reconstructed two-dimensional distributions of the first mode, which displayed two characteristic peaks, with the phase difference π rad between the oscillations in these peaks, agrees fairly well with the theoretically predicted structure of the lowest mode
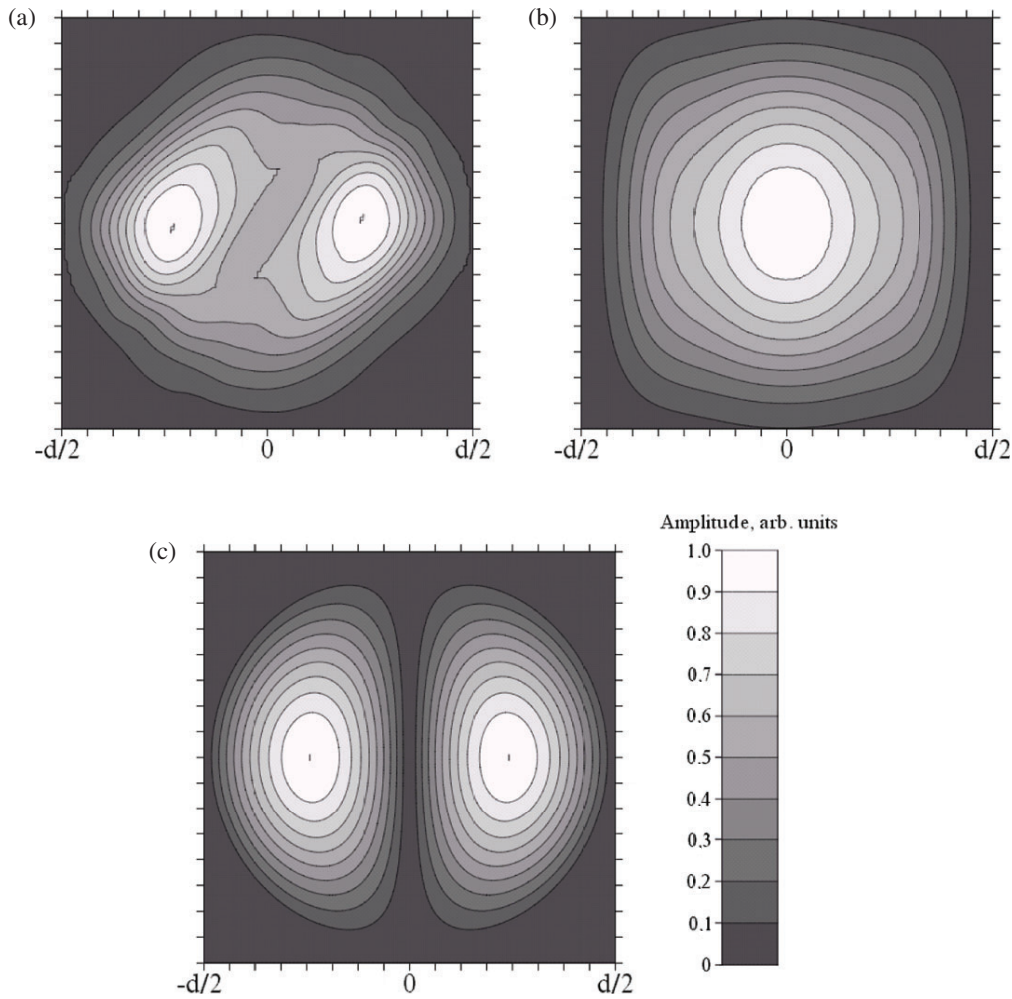
Figure 7. Reconstructed tomograms of the first and second oscillation modes (*a*) and (*b*), respectively, and the theoretically predicted structure of the mode (1, 1) (*c*).
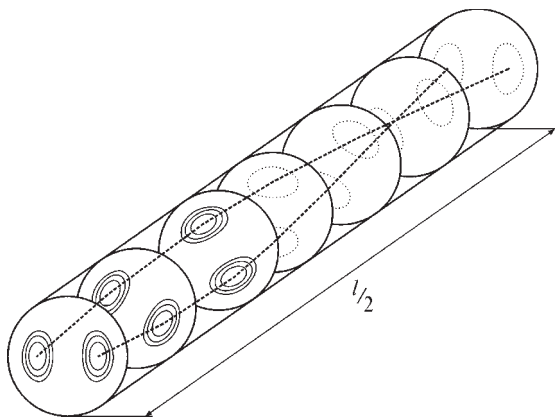

Figure 8. Three-dimensional structure of the first oscillation mode (schematically).

(1, 1), which is depicted in figure 7(*c*). A comparison between the tomograms of the first mode obtained in adjacent cross-sections of the discharge tube revealed a weak rotation of the observed characteristic structural features about the *z*-axis. The latter has allowed us to identify the three-dimensional structure of the first mode as a double helix with an estimated

pitch $l \simeq 50$–100 cm (see figure 8). The reasons for the weak rotation of the spatial structure of the first mode with displacement along the coordinate *z* cannot be explained within the framework of available theories [8, 12, 13] and were not examined in this work.

Reliable identification of the spatial structure of the second mode is difficult because the views in our experiments were few in number. Based on the distinct difference between projections obtained under different viewing angles, we may tentatively attribute the second frequency as belonging to the mode (1, 2) of model [8]. Although the model [8] predicts that the cross-sectional distributions of the mode (1, 2) should contain four maxima; in measured distributions, the two central maxima could merge together to give the experimentally observed three-peaked structure.

4. Conclusions

In this paper, we report on the first ever determination of the two-dimensional spatial structure of the two lowest modes of ion-acoustic oscillations in the continuous-wave ion argon laser plasma. The data obtained allows us to confidently state that the fundamental mode is the mode with $m = 1$ and $n = 1$,

whereas the second mode is most probably the mode with $m = 1$ and $n = 2$. Some problems still remain with the second mode, whose resolved structure has insufficient detail to allow its reliable identification. These problems can be solved using an experimental scheme capable of providing a larger number of views in the experiment and, hence, a better reconstruction quality.

The new approach, which in this study was used to measure cross-sectional distributions of the oscillation intensity in the discharge column, can be used to examine the spatial structure of oscillatory processes in other emissive media. After some modifications, it may also be used as a research tool in solid-state physics.

References

[1] Crawford F W 1961 *Phys. Rev. Lett.* **6** 663
[2] Zaitsev A A and Shvilkin B N 1967 *Sov. Phys.—Dokl.* **12** 68
[3] Donin V I 1972 *Sov. Phys. JETP* **35** 858
[4] Wang C P and Lin S C 1972 *J. Appl. Phys.* **43** 5068
[5] Gadetsky N P, Tkach Yu V, Sidelnikova A V and Zeidlits V P 1974 *Ukr. Fiz. Zh.* **19** 931
[6] Lüthi H R and Seelig W 1977 *J. Appl. Phys.* **48** 4922
[7] Alferov G N, Donin V I, Smirnov G I and Shapiro D A 1981 *Sov. J. Quantum Electron.* **11** 5
[8] Donin V I, Shapiro D A, Yakovin D V and Yatsenko A S 1988 *Phys. Lett.* A **126** 273
[9] Donin V I 1991 *High-Power Ion Gas Lasers* (Novosibirsk: Nauka)
[10] Babin S A, Donin V I and Kuklin A E 1991 *J. Phys. D: Appl. Phys.* **24** 7
[11] Donin V I, Ivanov V A and Yakovin D V 2001 *Tech. Phys.* **46** 400
[12] Woods L C 1965 *J. Fluid Mech.* **23** 315
[13] Ewald H N, Crawford F W and Self S A 1969 *Phys. Fluids* **12** 303
[14] Veretennikov V A, Koshevoi M O, Panferov N V, Pikalov V V, Rupasov A A, Semenov O G and Shikanov A S 1992 *Sov. J. Plasma Phys.* **18** 131
[15] Pickalov V V and Melnikova T S 1995 *Plasma Tomography* (Novosibirsk: Nauka)
[16] Ingesson L C and Pickalov V V 1996 *J. Phys. D: Appl. Phys.* **29** 3009
[17] Ivanov V A and Pickalov V V 2002 *Proc. IASTED Int. Conf. on Automation, Control and Information Technology (Novosibirsk, Russia, 10–13 June 2002)* (Anaheim-Calgary-Zurich: ACTA Press) p 480
[18] Webb C C 1968 *J. Appl. Phys.* **39** 5441
[19] Minerbo G N, Sanderson J G, van Hulsteyn D B and Lee P 1980 *Appl. Opt.* **19** 1723